Origin of Residual Stress in Arteries

Luca Cardamone[1], Jay D. Humphrey[2]
[1]*Department of Civil Engineering, University of Salerno, Italy*
E-mail: lcardamo@unisa.it

[2]*Department of Biomedical Engineering, Texas A&M University, USA*
E-mail: jhumphrey@tamu.edu

Keywords: Vascular development, Elastin, Aging, Hypertension, Residual stress, Opening angle.

SUMMARY. The structural protein elastin endows large arteries with unique biological functionality and mechanical integrity, hence its disorganization, fragmentation, or degradation can have important consequences on the progression and treatment of vascular diseases. There is, therefore, a need in arterial mechanics to move from materially uniform, phenomenological, constitutive relations for the wall to those that account for separate contributions of the primary structural constituents. In this paper, we employ a recently proposed constrained mixture model of the arterial wall and show that highly prestretched elastin contributes significantly to both the retraction of arteries that is observed upon transection and the opening angle that follows the introduction of a radial cut in an unloaded segment. We also show that the transmural distributions of elastin and collagen, compressive stiffness of collagen, and smooth muscle tone play complementary roles.

1 INTRODUCTION

Observations in the 1960s revealed that arteries retract when transected, thus suggesting the existence of an axial prestretch that defines the preferred length *in vivo*. Subsequent studies by [1], using elastase and collagenase to selectively remove structural components from the wall, demonstrated that nearly all axial prestretch in healthy arteries is due to the presence of intramural elastin, not collagen.

Findings in the 1960s revealed further that there exists "some degree of stress even when there is no distending pressure" in an artery [2]. Independent observations [3] confirmed the existence of residual stresses in arteries, which appear to arise from nonuniform growth and remodeling processes during development and can change in responses to disease or injury in maturity [4]. Experiments [5] using elastase, collagenase, and rapid freezing to selectively remove the three dominant structural constituents from the wall, showed that these residual stresses depend primarily on intramural elastin, not collagen or smooth muscle. Related to this finding, Zeller [6] suggested that net residual stresses in the wall likely depend on different residual stresses within individual constituents, with elastin having a residual tension and collagen a residual compression.

The existence of residual stress in an intact but traction-free excised arterial segment suggests a net compressive stress in the inner wall and a net tensile stress in the outer wall, which is captured easily by both standard stress analyses [7] and computational models of arterial growth [8]. Such models have been based on materially uniform, phenomenological, constitutive relations, however, and thus have not been capable of assessing the potential roles of individual constituents or how they are formed during development or maturity. The goal of this paper, therefore, is to employ a recently proposed materially nonuniform, structurally motivated, constrained mixture model of the arterial wall to study the means by which elastin plays such an important role in the development of axial

prestress and residual stress in the normal arterial wall, two key factors in mechanical homeostasis.[1] We submit further that the constrained mixture model employed herein can be used to build residual stresses into patient-specific computational models without the need to define spatially and temporally changing opened configurations [9] which could be particularly advantageous in modeling complex geometries.

2 METHODS

2.1 Theoretical Framework

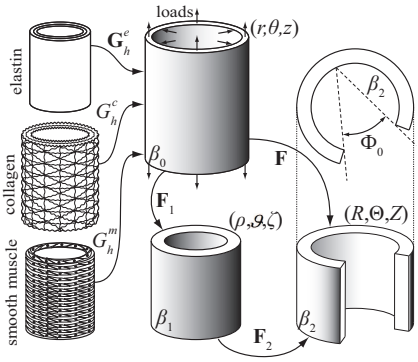

Figure 1: Schema of the constrained mixture model of an arterial segment consisting of elastin, multiple families of collagen fibers, and smooth muscle.

In contrast to usual formulations, which use the "stress-free" configuration as a reference [9], we use the current, stressed configuration as a computational reference. Hence, we prescribe the kinematics for an idealized axisymmetric artery via two successive motions (Figure 1): mappings of material points from the *in vivo* configuration β_0 (r, θ, z), associated with the finite extension and inflation of an intact cylindrical segment, to an intact but traction-free excised configuration β_1 (ρ, ϑ, ζ) and then to a nearly stress-free, radially-cut configuration β_2 (R, Θ, Z). The deformation gradients for these motions are given by

$$\mathbf{F}_1 = \mathrm{diag}\left[\frac{\partial \rho}{\partial r}, \frac{\rho}{r}, \frac{1}{\lambda}\right], \ \mathbf{F}_2 = \mathrm{diag}\left[\frac{\partial R}{\partial \rho}, \frac{(\pi - \Phi_0)\, R}{\pi \rho}, \frac{1}{\Lambda}\right], \tag{1}$$

with Φ_0 and Λ the residual stress related opening angle and axial stretch, respectively, and λ the additional axial stretch related primarily to the *in vivo* "prestretch". The total deformation gradient is thus computed via $\mathbf{F} = \mathbf{F}_2\mathbf{F}_1$ and incompressibility is assumed to hold during transient motions, hence $\det \mathbf{F} = 1$ herein. The Cauchy stress $\boldsymbol{\sigma}$ associated with either the first ($\mathbf{F} = \mathbf{F}_1$ with $\mathbf{F}_2 = \mathbf{I}$) or the total ($\mathbf{F} = \mathbf{F}_2\mathbf{F}_1$) motion can be computed via

$$\mathrm{div}\boldsymbol{\sigma} = \mathbf{0}, \quad \boldsymbol{\sigma} = -p\mathbf{I} + \frac{\partial W}{\partial \mathbf{F}}\mathbf{F}^{\mathrm{T}} + \boldsymbol{\sigma}^{\mathrm{act}}, \tag{2}$$

where p is a Lagrange multiplier that enforces incompressibility, W is the net strain energy function for the passive behavior of the wall, and $\boldsymbol{\sigma}^{\mathrm{act}}$ accounts for smooth muscle activity. Consistent with

[1] By prestress, we mean stress in a body under a normal state of loading in the absence of what might be thought of as additional, perturbing loads. By residual stress, we mean stresses that exist independent of applied loads, which must self-equilibrate by definition.

[10], we employ a rule-of-mixtures constitutive relation for the passive response, namely

$$W = \phi^e W^e\left(\mathbf{F}^e\right) + \sum_{c=1}^{4} \phi^c W^c\left(\lambda^c\right) + \phi^m W^m\left(\lambda^m\right), \tag{3}$$

where ϕ^i are mass fractions for each structurally significant constituent and W^i are individual strain energy functions ($i = e$ for amorphous elastin, $i = c = 1, 2, 3, 4$ for four fibers of collagen fibers, and $i = m$ for circumferentially oriented passive smooth muscle). In equation (3) $\mathbf{F}^e$, λ^c, and λ^m represent the elastin deformation gradient, the collagen fiber stretch and the smooth muscle stretch respectively. These quantities are defined with respect to individual stress-free configurations (see Figure 1). The active smooth muscle contribution is given by [11]

$$\boldsymbol{\sigma}^{\mathrm{act}} = T_{\mathrm{M}}\left(1 - e^{C^2}\right)\lambda^m\left[1 - \left(\frac{\lambda_{\mathrm{M}} - \lambda^m}{\lambda_{\mathrm{M}} - \lambda_0}\right)^2\right]\mathbf{e}_\theta \otimes \mathbf{e}_\theta, \tag{4}$$

where T_{M}, λ_{M}, and λ_0 are the maximum (mass averaged) stress, the stretch at which the active force generation is maximum, and the stretch at which the active force generation is zero, respectively. Clearly, therefore, the active stress depends on a constrictor concentration C and the muscle fiber stretch. Whereas elastin is assumed to be distributed isotropically, families of parallel collagen fibers are assumed to be oriented axially, circumferentially, and diagonally [12], and the smooth muscle cells are assumed to be oriented circumferentially (cf. Figure 1), the constituent stretch ratios in appropriate directions λ^i are computed based on individual stress-free configurations for each constituent and the constrained mixture theory is employed to relate their kinematics to overall vessel motion [13, 10].

The key observation, consistent with what suggested in [6], is that elastin is produced during the perinatal period and is normally stable thereafter [14, 15], thus it undergoes large multiaxial stretches as the artery grows to the adult configuration β_0. On the other hand, collagen and smooth muscle turn over continuously throughout life [15] and we assume that they are deposited at a preferred stretch during maturity. These assumptions result in higher "prestretches" in elastin than in collagen and smooth muscle in maturity.

Equilibrium of the *in vivo* configuration β_0, both local and global (integral) forms, requires

$$\int_{r_i}^{r_a} (\sigma_{\theta\theta} - \sigma_{rr})\frac{\mathrm{d}\varrho}{\varrho} = P,\ 2\pi\int_{r_i}^{r_a} \sigma_{zz}\varrho \mathrm{d}\varrho = f, \tag{5}$$

where r_i and r_a denote intimal and adventitial radii in β_0 and P and f are the *in vivo* luminal pressure and axial force, respectively. In order to ensure radial equilibrium, with the given *in vivo* luminal pressure P, equation $(5)_1$ is solved for the adventitial radius r_a while the axial force f is computed explicitly from equation $(5)_2$. In this way, in all the simulations, the material parameters, the intimal radius, and the luminal pressure can be kept constant regardless the features of the distribution of constituents prestretches and mass fractions, while a slight variation in the outer radius (less than 0.1% of the reference value reported in Table 1 for the cases simulated) preserves the radial equilibrium.

Equilibrium of the unloaded configuration β_1 similarly requires

$$\int_{\rho_i}^{\rho_a} (\sigma_{\vartheta\vartheta} - \sigma_{\rho\rho})\frac{\mathrm{d}\varrho}{\varrho} = 0,\ \int_{\rho_i}^{\rho_a} \sigma_{\zeta\zeta}\varrho \mathrm{d}\varrho = 0, \tag{6}$$

Table 1: Parameter values used for the normal human basilar artery [10].

Prestretches and Elastic Parameters
$G^e_{h\theta} = G^e_{hz} = 1.4$, $G^e_{hr} = 1/\left(G^e_{h\theta}G^e_{hz}\right)$♣, $G^m_h = 1.2$, $G^c_h = 1.08$
$c^e = 237.6$ kPa, $c^m_2 = 36.5$ kPa, $c^c_2 = 560.4$ kPa, $c^m_3 = 3.5$, $c^c_3 = 22.0$
Mass Fractions (dry weight)
$\phi^e = 0.02$, $\phi^m = 0.76$, $\phi^c = 0.22$
Muscle Activation Parameters
$T_{\rm M} = 150$ kPa$\times\phi^m$, $\lambda_{\rm M} = 1.1$, $\lambda_0 = 0.4$, $C_B = 0.68$
In Vivo Geometry
$r_i = 1.42$ mm, $r_a \approx 1.60$ mm♠

♣uniform elastin prestretches for the reference case, used if not specified otherwise.
♠slightly dependent on the distribution of constituents mass fraction and prestretch, this reference value corresponds to uniform distribution of constituents and $G^e_{h\theta} = G^e_{hz} = 1.4$.

where ρ_i and ρ_a denote intimal and adventitial radii in β_1. The two global equations can be solved to determine the inner radius ρ_i and the net *in vivo* axial prestretch λ for prescribed material properties and distribution of constituents prestretch and mass fraction.

Finally equilibrium of the radially-cut configuration β_2 can be satisfied via the following [8]

$$\int_{R_i}^{R_a} (\sigma_{\Theta\Theta} - \sigma_{RR})\frac{\mathrm{d}\varrho}{\varrho} = 0, \int_{R_i}^{R_a} \sigma_{ZZ}\varrho\mathrm{d}\varrho = 0, \int_{R_i}^{R_a} \sigma_{\Theta\Theta}\varrho\mathrm{d}\varrho = 0, \tag{7}$$

where R_i and R_a denote intimal and adventitial radii in β_2. Note that the additional global equilibrium equation enforces zero applied moments on the radially-cut section. The three global equations can be solved to determine the inner radius R_i, the net *in vivo* axial prestretch $\Lambda\lambda$, given λ from above, and the residual stress related opening angle Φ_0 for prescribed material properties and distribution of constituents prestretch and mass fraction.

2.2 Simulation Strategy

For illustrative purposes, we let the mechanical behavior of the elastin-dominated amorphous matrix be isotropic and described by a neo-Hookean strain energy density function [16, 17]

$$W^e = \frac{c^e}{2}\left((\lambda^e_r)^2 + (\lambda^e_\theta)^2 + (\lambda^e_z)^2 - 3\right), \tag{8}$$

where c_1 is a material parameter (Table 1) and λ^e_i (with $i = r, \theta, z$) are the principal stretches of the elastin, whose deformation gradient is given by $\mathbf{F}^e = \mathbf{F}\mathbf{G}^e_h$ (cf. equation 3). $\mathbf{F}^e = \mathbf{G}^e_h$ in the normal configuration (i.e., we do not delineate deposition stretches during development for elastin and its subsequent stretch due to normal growth). Similarly, let the behavior of the passive smooth muscle and collagen fibers be described by exponential forms [18]

$$W^m = \frac{c^m_2}{4c^m_3}\left[e^{c^m_3\left((\lambda^m)^2-1\right)^2} - 1\right], \quad W^c = \frac{c^c_2}{4c^c_3}\left[e^{c^c_3\left((\lambda^c)^2-1\right)^2} - 1\right], \tag{9}$$

where $c^m_2,\ c^m_3,\ c^c_2,\ c^c_3$ are material parameters (Table 1).

A fundamental assumption is that each structurally significant constituent can possess a unique natural configuration. That is, individual constituents need not be unstressed when the overall tissue is unstressed. It can be shown [13] that constituent-level stretches (e.g., λ^e_r, λ^e_θ, λ^e_z, λ^c, λ^m) can be

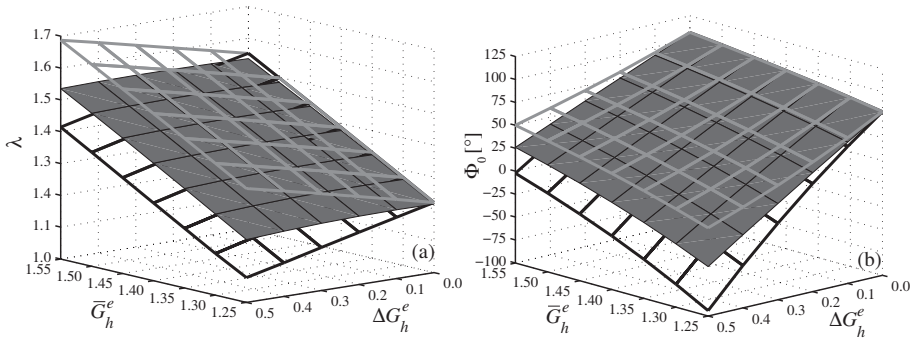

Figure 2: (a) Overall axial stretch from the intact, unloaded configuration and (b) opening angle due to a radial cut, each for elastin prestretches distributed linearly through the thickness. Solid surfaces are for the intact vessel whereas gray and black framed surfaces show results for inner and outer rings, respectively.

related to the tissue-level stretches (e.g., λ_r, λ_θ, λ_z) via homeostatic deposition stretch (e.g., G^e_{hr}, $G^e_{h\theta}$, G^e_{hz}, G^c_h, G^m_h).

Equations $(5)_1$, (6), and (7) were solved using a Newton-Raphson method to determine the yet unknown kinematic parameters (i.e., r_a in β_0, λ and ρ_i in β_1, and Φ_0, $\Lambda\lambda$, and R_i in β_2).

3 RESULTS

Henceforth, we focus on the basilar artery, one of the primary arteries suppling blood to the brain.

3.1 Uniform versus Linear Distributions of Elastin Prestretches

Recall, that elastin is produced primarily during the late prenatal and early postnatal periods, starting in the inner layer of the wall and moving outward, and it is very stable [14, 15]. Hence, it is reasonable to assume that elastin deposited earlier (inner layers) experiences higher prestretches in the final *in vivo* configuration since it "remembers" a smaller original configuration and is stretched more during arterial enlargement compared to the elastin deposited later (outer layers).

Given this hypothesis, we compared a uniform versus a linear distribution of elastin prestretches for different mean values $\overline{G}^e_h \equiv \overline{G}^e_{h\theta} \equiv \overline{G}^e_{hz}$ or for differences ΔG^e_h between the highest prestretch at the inner wall $G^e_h(r_i) = G^e_{h\theta}(r_i) = G^e_{hz}(r_i)$ and the lowest one at the outer wall $G^e_h(r_a) = G^e_{h\theta}(r_a) = G^e_{hz}(r_a)$ (i.e., $\Delta G^e_h = G^e_h(r_i) - G^e_h(r_a)$). Figure 2 shows the predicted overall axial prestretch and opening angle as a function of assumed values for both $\overline{G}^e_h$ and ΔG^e_h for the intact vessel (solid surfaces) as well as for inner (gray frame) and outer (black frame) rings obtained via a circumferential cut at the mid-wall in the *in vivo* configuration [19]. As is evident from Figure 2(a), the unloaded length decreased with increases in the mean value of elastin prestretches $\overline{G}^e_h$ but was nearly insensitive to transmural differences ΔG^e_h. This result is explained easily by noting that the unloaded length is dictated by an equilibrium between compression of collagen and smooth muscle and tension in the elastin; increasing the mean elastin prestretch shifted the equilibrium towards a greater compression of collagen and muscle and thus towards a shorter unloaded length. The unloaded length for the inner and outer rings increased and decreased, respectively, with ΔG^e_h because the mean elastin prestretch increased in the inner and decreased in the outer ring when the magnitude of the distribution increased.

Figure 2(b) shows that the opening angle depended strongly on both the mean value and the transmural distribution of elastin prestretches, but it was more sensitive to the latter. For $\Delta G^e_h = 0$

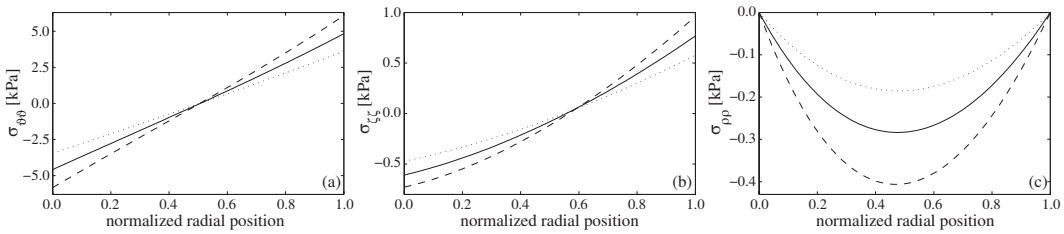

Figure 3: Residual stresses in the intact, unloaded configuration β_1 of the whole vessel for uniformly distributed prestretch of elastin: $\overline{G}_h^e = 1.55$ (dashed), $\overline{G}_h^e = 1.40$ (solid), and $\overline{G}_h^e = 1.25$ (dotted).

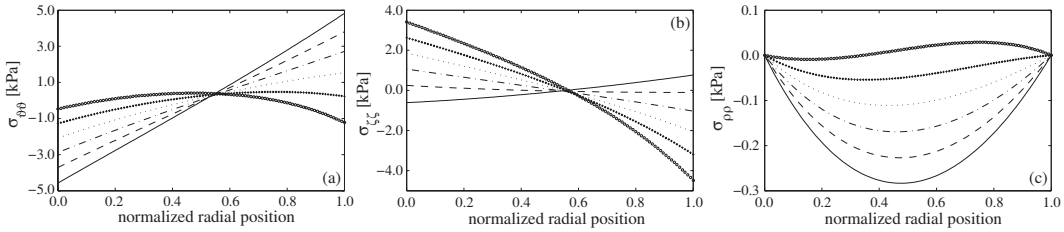

Figure 4: Residual stresses in the intact, unloaded configuration β_1 of the whole vessel for a fixed mean elastin prestretch $\overline{G}_h^e = 1.40$, but different linear transmural distribution in prestretches: $\Delta G_h^e = 0.0$ (solid), $\Delta G_h^e = 0.1$ (dashed), $\Delta G_h^e = 0.2$ (dash-dotted), $\Delta G_h^e = 0.3$ (dotted), $\Delta G_h^e = 0.4$ (+), and $\Delta G_h^e = 0.5$ (∘).

(i.e., a homogeneous material), both the whole vessel and each ring obtained from the circumferential cut opened to the same angle because the unloaded radially-cut, configuration was stress free and the circumferential cut had no further effect. For nonuniform prestretches ($\Delta G_h^e > 0$), however, the inner (outer) ring experienced larger (smaller) opening angles because the mean prestretch was higher (lower) than in the intact vessel; this is consistent with reports by [19] and [5].

As is evident from Figure 3(a), larger opening angles for a whole vessel having greater mean elastin prestretches can be explained by the increased circumferential residual stress in the intact unloaded configuration, which leads to a larger opening moment – see equation $(7)_3$. Figure 3 also shows that increasing the mean elastin prestretches increased the residual stresses in the unloaded configuration, but these residual stresses were not influenced qualitatively by the value of $\overline{G}_h^e$. In contrast, Figure 4 shows that the magnitude of the transmural distribution in prestretch ΔG_h^e influenced the transmural distribution of the residual stresses qualitatively. Comparison of Figures 3 and 4 shows that variations in ΔG_h^e influence the residual stresses in the intact unloaded configuration much more than $\overline{G}_h^e$.

Consistent with the unloaded configuration depending mainly on the mean prestretch of elastin, not its transmural distribution, increasing ΔG_h^e led to less compression of inner layers and less tension in outer layers, and thus a strong reduction of the opening angle. For high values of ΔG_h^e, the opening moment actually changed sign (Figure 4(a)) the vessel closed on itself after introducing the radial cut (Figure 2(b)). Uniform distributions of prestretches never led to negative opening angles, yet such results have been observed in arteries [20].

Figure 5 shows that introducing a single radial cut was sufficient to release all residual stresses only if the material was homogeneous, otherwise the vessel was not stress free in the radially-cut, unloaded configuration.

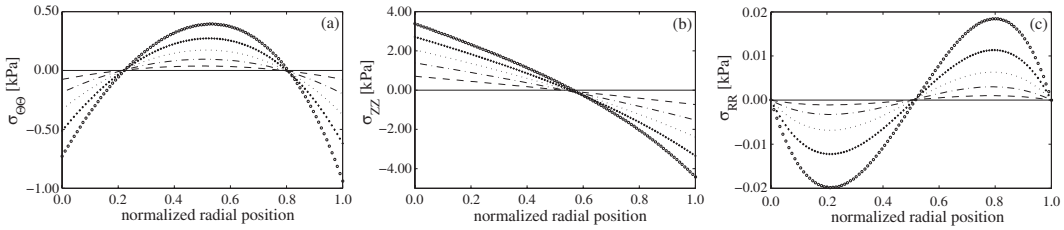

Figure 5: Residual stresses in the radially-cut configuration β_2 for fixed mean elastin prestretch $\overline{G}_h^e = 1.40$, but different linear transmural distribution in prestretches: $\Delta G_h^e = 0.0$ (solid), $\Delta G_h^e = 0.1$ (dashed), $\Delta G_h^e = 0.2$ (dash-dotted), $\Delta G_h^e = 0.3$ (dotted), $\Delta G_h^e = 0.4$ (+), and $\Delta G_h^e = 0.5$ (∘).

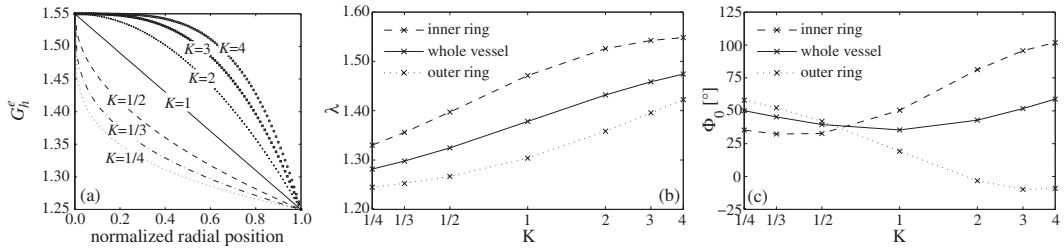

Figure 6: (a) Transmural distribution of G_{hz}^e and $G_{h\theta}^e$ for different values of K as given by equation (10) for $G_h^e(r_i) = 1.55$ and $G_h^e(r_a) = 1.25$. (b) Overall axial stretch and (c) opening angle as functions of K.

3.2 Nonlinear Distribution of Elastin Prestretches

The assumption of a linear distribution of elastin prestretches through the wall implies that the "rate of deposition" is somehow synchronized with arterial development. To study different hypotheses for the rate of deposition of elastin, we considered the following distributions of prestretch in the axial and circumferential directions

$$G_h^e(r) = G_h^e(r_i) + [G_h^e(r_a) - G_h^e(r_i)] \left(\frac{r - r_i}{r_a - r_i} \right)^K , \tag{10}$$

where K is a parameter governing the "deposition rate". $K > 1$ models consequences of a higher rate of deposition in early stages of development such that all inner layers experience similar elastin prestretches in maturity (Figure 6(a)). $K < 1$ models a slower rate in early development such that the inner layers experience a strong gradient in elastin prestretch while the outer layers vary less. $K = 1$ recovers the linear distribution. We studied potential consequences of the rate of deposition by fixing the prestretches in the *intima* ($G_h^e(r_i) = 1.55$) and *adventitia* ($G_h^e(r_a) = 1.25$) and varying the rate parameter K.

The net unloaded axial stretch and the opening of the two rings obtained from both circumferential and radial cuts are shown in panels 6(b,c) as a function of K. The unloaded length decreased monotonically with K for the whole vessel and both rings. This is consistent with our other findings because increasing K leads to an increased mean prestretch and thus an increased retraction upon unloading. Moreover, the order $\lambda_{in} < \lambda < \lambda_{out}$ was preserved regardless of the value of K because the mean elastin prestretch was higher in the inner ring than in the whole vessel and it was higher in the whole vessel than in the outer ring.

Figure 6(c) shows that the opening angle for the intact vessel was smallest for $K = 1$ and those

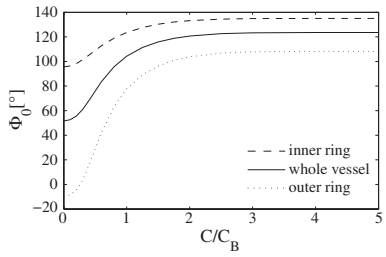

Figure 7: Opening angle as a function of the normalized constrictor concentration for $G_h^e(r_i) = 1.55$, $G_h^e(r_a) = 1.25$, $K = 3$.

for the inner and outer rings differed most when $K \geq 1$. $K > 1$ led, consistently with the aforementioned observations for linearly distributed prestretches, to larger opening angles compared to the whole vessel. In contrast, the outer layers experienced a large transmural variation of prestretch with radial position, which led to a negative opening angle (such angles have been reported for different arteries in [20]). For $K < 1$ the high level of inhomogeneity within the inner ring overwhelmed the effect of mean elastin prestretch, thus the inner ring opened less than the whole vessel while the small inhomogeneity in the outer layer dominated the effect of the small mean prestretch and its opening angle was larger compared to the whole vessel. The opening angles for both inner and outer rings reinforce the finding, shown in Figure 2, that the distribution of elastin prestretch dominates the effect of its mean value. $K \geq 1$ are the most realistic results, predicting higher opening angles for the inner ring compared to the outer ring [19]. Moreover, considering that most layers of elastin are deposited and cross-linked during early development, the distribution of elastin prestretches given by $K \geq 1$ could be the most representative.

3.3 Brief Summary

Based on results presented thus far, it appears that a nonuniform distribution of elastin prestretch with $\Delta G_h^e > 0$ and $K \geq 1$ is the most realistic – it yields a nearly uniform stress distribution through the thickness at any pressure during the cardiac cycle (not shown) and it gives a larger opening angle for the inner ring than the outer ring following a circumferential cut (Figure 6(c)). Moreover this type of distribution could find its explanation in the developmental process as discussed earlier. For these reasons we assume $G_h^e(r_i) = 1.55$, $G_h^e(r_a) = 1.25$, and $K = 3$ (see panel 6(a)) in the remaining simulations.

3.4 Effect of Smooth Muscle Tone

All prior computations for both the intact and the radially-cut unloaded configurations were performed with no smooth muscle tone (i.e., passive). Nevertheless, muscle tone can influence the opening angle because it modifies the distributions of both *in vivo* and residual stresses. Figure 7 shows that an increased smooth muscle tone increased the opening angle, consistent with data for rat aorta reported by [21] and [22] as well as with simulations in [11]. Moreover, our simulations showed that the opening angle of the inner (outer) ring is more (less) sensitive to smooth muscle contraction than that for the whole vessel.

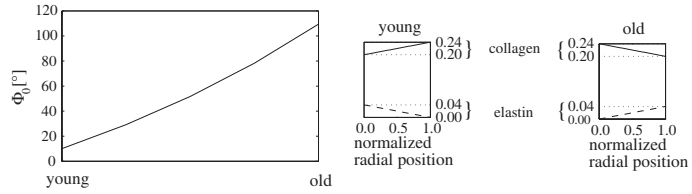

Figure 8: Effect of one aspect of aging on the opening angle with $G_h^e(r_i) = 1.55$, $G_h^e(r_a) = 1.25$, $K = 3$. Young: $\phi^e(r_i) = 0.04$, $\phi^e(r_a) = 0$, $\phi^c(r_i) = 0.2$, and $\phi^c(r_a) = 0.24$. Old: $\phi^e(r_i) = 0$, $\phi^e(r_a) = 0.04$, $\phi^c(r_i) = 0.24$, and $\phi^c(r_a) = 0.2$.

3.5 Aging

It is reported in [23] that transmural gradients of elastin and collagen mass fractions reverse with age in human aorta. In particular, the amount of elastin decreases and that of collagen increases from the *intima* to the *adventitia* in young individuals; conversely, in aging the amount of intimal elastin decreases while that of collagen increases and adventitial elastin increases while collagen decreases, all without significantly changing total scleroprotein through the wall (i.e., the sum of elastin plus collagen was reported to be nearly uniform and not a function of age). Later studies on human aortas [24] showed further that there is an increase in the opening angle with age.

We simulated effects of the redistribution of collagen and elastin in the wall reported in [23] by assuming the linear distributions depicted in Figure 8 while keeping uniform the total mass fraction of the scleroprotein (i.e., $\varphi^e(r) + \varphi^c(r) = 0.24\ \forall r \in [r_i, r_a]$). The simulations confirmed that a gradual reversal in the gradients of elastin and collagen (as in aging) causes a monotonic increase in opening angle.

References

[1] P. B. Dobrin, T. H. Schwarcz, and R. Mrkvicka, "Longitudinal retractive force in pressurized dog and human arteries," *J. Surg. Res.*, vol. 48, pp. 116–120, 1990.

[2] D. H. Bergel, *The visco-elastic properties of the arterial wall*. PhD thesis, University of London, UK, 1960.

[3] Y. C. Fung, *What principle governs the stress distribution in living organism?*, pp. 1–13. Beijing: Science Press, 1983.

[4] Y. C. Fung, "What are residual stresses doing in our blood vessels?," *Ann. Biomed. Eng.*, vol. 19, pp. 237–249, 1991.

[5] S. E. Greenwald, J. E. Moore, A. Rachev, T. P. C. Kane, and J.-J. Meister, "Experimental investigation of the distribution of residual strains in the artery wall," *J. Biomech. Eng.*, vol. 126, pp. 371–381, 1997.

[6] P. J. Zeller and T. C. Skalak, "Contribution of individual structural components in determining the zero-stress state in small arteries," *J. Vasc. Res.*, vol. 35, pp. 8–17, 1998.

[7] C. J. Chuong and Y. C. Fung, "On residual stress in artery," *J. Biomech. Eng.*, vol. 108, pp. 189–192, 1986.

[8] L. A. Taber and J. D. Humphrey, "Stress-modulated growth, residual stress, and vascular heterogeneity," *J. Biomech. Eng.*, vol. 123, pp. 528–535, 2001.

[9] V. Alastrué, E. Peña, M. A. Martínez, and M. Doblaré, "Assessing the use of the "opening angle method" to enforce resdidual stresses in patient–specific arteries," *Ann. Biomed. Eng.*, vol. 35, pp. 1821–1837, 2007.

[10] A. Valentín, L. Cardamone, S. Baek, and J. D. Humphrey, "Complementary vasoactivity and matrix remodeling in arterial adaptations to altered flow and pressure," *J. Roy. Soc. Interface*, vol. 6, pp. 293–306, 2009.

[11] A. Rachev and K. Hayashi, "Theoretical study of the effects of vascular smooth muscle contraction on strain and stress distributions in arteries," *Ann. Biomed. Eng.*, vol. 27, no. 4, pp. 459–468, 1999.

[12] B. K. Wicker, H. P. Hutchens, Q. Wu, A. T. Yeh, and J. D. Humphrey, "Normal basilar artery structure and biaxial mechanical behavior," *Comput. Meth. Biomech. Biomed. Eng.*, vol. 11, no. 5, pp. 539–551, 2008.

[13] S. Baek, K. R. Rajagopal, and J. D. Humphrey, "A theoretical model of enlarging intracranial fusiform aneurysms," *J. Biomech. Eng.*, vol. 128, no. 1, pp. 142–9, 2006.

[14] E. C. Davis, "Elastic lamina growth in the developing mouse aorta," *J. Histochem. Cytochem.*, vol. 43, pp. 1115–1123, 1995.

[15] B. L. Langille, "Arterial remodeling: relation to hemodynamics," *Can. J. Physiol. Pharmacol.*, vol. 74, no. 7, pp. 834–41, 1996.

[16] K. Dorrington and N. McCrum, "Elastin as a rubber," *Biopolymers*, vol. 16, no. 6, pp. 253–264, 1977.

[17] G. A. Holzapfel, T. C. Gasser, and R. W. Ogden, "A new constitutive framework for arterial wall mechanics and a comparative study of material models," *J. Elasticity*, vol. 61, pp. 1–48, 2000.

[18] E. Nevo and Y. Lanir, "Strucutural finite deformation model of the left ventricle during diastole and systole," *J. Biomech.*, vol. 111, pp. 342–349, 1989.

[19] J. Vossoughi, H. Hedjazi, and F. S. I. Borris, "Intimal residual stress and strain in large arteries," pp. 434–437, New York: ASME, 1993.

[20] Y. C. Fung, *Biomechanics: Motion, Flow, Stress, and Growth*. New York: Springer–Verlag, 1993.

[21] T. Matsumoto, M. Tsuchida, and M. Sato, "Change in intramural strain distribution in rat aorta due to smooth muscle contraction and relaxation," *Am. J. Physiol.*, vol. 271, pp. H1711–1716, 1996.

[22] P. Fridez, *The role of vascular smooth muscle in biomechanical adaptation of the arterial wall to induced hypertension*. PhD thesis, Swiss Federal Institute of Technology, 2000.

[23] S. A. Feldman and S. Glagov, "Transmural collagen and elastin in human aortas: reversal with age," *Atherosclerosis*, vol. 13, pp. 385–394, 1971.

[24] A. Saini, C. L. Berry, and S. E. Greenwald, "The effect of age and sex on residual stress in the aorta," *J. Vasc. Res.*, vol. 32, pp. 398–405, 1995.